Acta Oceanol. Sin., 2021, Vol. 40, No. 8, P. 65–77
https://doi.org/10.1007/s13131-021-1864-5
http://www.aosocean.com
E-mail: ocean2@hyxb.org.cn

Spatiotemporal variations in the organic carbon accumulation rate in mangrove sediments from the Yingluo Bay, China, since 1900

Yao Zhang[1, 2], Xianwei Meng[2, 3*], Peng Xia[2], Jun Zhang[1, 2], Dahai Liu[2], Zhen Li[4], Wanzhu Wang[2]

[1] College of Marine Geosciences, Ocean University of China, Qingdao 266003, China

[2] First Institute of Oceanography, Ministry of Natural Resources, Qingdao 266061, China

[3] Laboratory for Marine Geology and Environment, Pilot National Laboratory for Marine Science and Technology (Qingdao), Qingdao 266061, China

[4] School of Earth and Ocean Sciences, University of Victoria, British Columbia V8W2Y2, Canada

Received 23 December 2020; accepted 24 March 2021

Abstract

Mangroves can not only provide multiple ecosystem service functions, but are also efficient carbon producers, capturers, and sinks. The estimation of the organic carbon accumulation rate (OCAR) in mangrove sediments is fundamental for elucidating the role of mangroves in the global carbon budget. In particular, understanding the past changes in the OCAR in mangrove sediments is vital for predicting the future role of mangroves in the rapidly changing environment. In this study, three dated sediment cores from interior and fringe of mangroves in the Yingluo Bay, China, were used to reconstruct the spatiotemporal variations of the calculated OCAR since 1900 in this area. The increasing OCAR in the mangrove interior was attributed to mangrove flourishment induced by climate change characterized by the rising temperature. However, in the mangrove fringe, the strengthening hydrodynamic conditions under the sea level rise were responsible for the decreasing OCAR, particularly after the 1940s. Furthermore, the duration of inundation by seawater was the primary factors controlling the spatial variability of the OCAR from the mangrove fringe to interior, while the strengthened hydrodynamic conditions after the 1940s broke this original pattern.

Key words: spatiotemporal variation, organic carbon accumulation rate, organic carbon source, mangrove development, temperature, hydrologic conditions

Citation: Zhang Yao, Meng Xianwei, Xia Peng, Zhang Jun, Liu Dahai, Li Zhen, Wang Wanzhu. 2021. Spatiotemporal variations in the organic carbon accumulation rate in mangrove sediments from the Yingluo Bay, China, since 1900. Acta Oceanologica Sinica, 40(8): 65–77, doi: 10.1007/s13131-021-1864-5

1 Introduction

Mangroves, exclusive ligneous plants occupying the intertidal zone in tropical/subtropical regions, provide multiple ecosystem services (Duke et al., 2007; Nellemann et al., 2009; Hatje et al., 2021). More importantly, mangrove forests play a disproportionately important role in global carbon cycling, and are key blue carbon sinks that can contribute to climate change mitigation (Jennerjahn and Ittekkot, 2002; Jennerjahn, 2012; Duarte et al., 2005; Duke et al., 2007; Alongi, 2014; Duarte, 2017; Sasmito et al., 2020).

To precisely elucidate the role of mangroves in the global carbon budget, the measurement of the organic carbon accumulation rate (OCAR) in mangrove sediments has attracted increasing public attention (Duarte et al., 2005; Kristensen et al., 2008; Breithaupt et al., 2012; Kusumaningtyas et al., 2019). Sediments (soils) are the most effective and largest carbon sink in mangrove ecosystems due to their capability to bury and preserve carbon under anoxic conditions induced by frequent tidal inundation (Kristensen et al., 2008). Moreover, unlike measuring carbon storage, the OCAR addresses the question of how much OC is sequestered in a specified period, quantifies the ongoing sink capacity, and subsequently aids in resolving the other aspects of system-scale carbon budgets, such as import, export, and remineralization (Breithaupt et al., 2012; Arias-Ortiz et al., 2018). The current calculated global average OCAR in mangroves (mean: 179.6 g/(m^2·a), according to C) is approximately 20 times larger than that of terrestrial forest ecosystems (Mcleod et al., 2011; Alongi, 2020), further highlighting the critical role of mangroves in the global carbon cycle.

However, there are still some key aspects and deficiencies in OCAR studies in mangrove sediments. (1) The OCAR can be various and site-specific in an individual same mangrove forest under the function of several interrelated factors, such as forest quality and the hydrological and geomorphological conditions (Alongi, 2020; Hatje et al., 2021; Matos et al., 2020). Therefore, surveys at different locations are indispensable and key for comprehensively assessing the carbon dynamics in mangrove ecosystems. (2) Understanding the past changes in OCAR is important for assessing the future role of mangroves in the rapidly changing environment (Jennerjahn, 2012; Hapsari et al., 2017). Many researchers only focused on the average OCAR in mangrove studies (Tateda et al., 2005; Yang et al., 2014; MacKenzie et al.,

Foundation item: The National Natural Science Foundation of China under contract Nos 41976068 and 41576061.
*Corresponding author, E-mail: mxw@fio.org.cn

2016). The variations in OCAR and their influencing factors over time are poorly understood (Cuellar-Martinez et al., 2020). (3) A 100 a time span is the most effective standard for long term OCAR studies in coastal wetlands (Breithaupt et al., 2014). However, the time spans of some studies were insufficient, or sediment cores lacked reasonable chronological frameworks (i.e., poor or uncorrected ^{210}Pb results), all of which caused imprecise OCAR estimation (Kusumaningtyas et al., 2019). (4) Few studies have linked the variations in carbon accumulation and carbon sources, particularly for mangrove-derived OC, which is crucial for evaluating the effectiveness of mangroves as blue carbon sinks (Kusumaningtyas et al., 2019; Matos et al., 2020).

Here, using three sediment cores reliably dated by ^{210}Pb chronology from different geomorphic settings in the Yingluo Bay, China, this study reconstructed the spatiotemporal variations in the calculated OCAR since 1900 in this area and discussed the factors controlling these variations. This study would be beneficial for evaluating the function of mangrove ecosystems in the carbon cycle and provides a theoretical reference for national carbon strategies in the future.

2 Materials and methods

2.1 *Study area and sampling sites*

The Yingluo Bay, located in the northern Beibu Gulf, Guang Xi Zhuang Autonomous Region, and adjacent to the Leizhou Peninsula, China, contains the Shankou Mangrove National Nature Reserve (SMNNR; 21°28′–21°37′N, 109°37′–109°47′E) for mangroves (Fig. 1), covering a total area of 80 km^2 and stretching along the coast for 50 km. There are 21 mangrove species in the area, that exhibited a zonal distribution from the dike (*Excoecaria agallocha*) to the upper (*Bruguiera gymnorrhiza* and *Rhizophora stylosa*), middle (*Kandelia candel* and *Aegiceras corniculatum*), and lower (*Avicennia marina*) tidal flats (Li et al., 2008). The landforms consist of mangrove flats, tidal flats, and a tidal creek system. The sediments are primarily composed of silty clay and sandy-silty clay. The reserve is located far away from the estuary, and terrestrial materials are transported to the mangrove swamps by the Beibu Gulf circulation (Xia et al., 2015).

The study area experiences a tropical monsoonal climate with a pronounced maritime influence. The mean annual temperature is 22.4°C, with maximum and minimum temperatures of

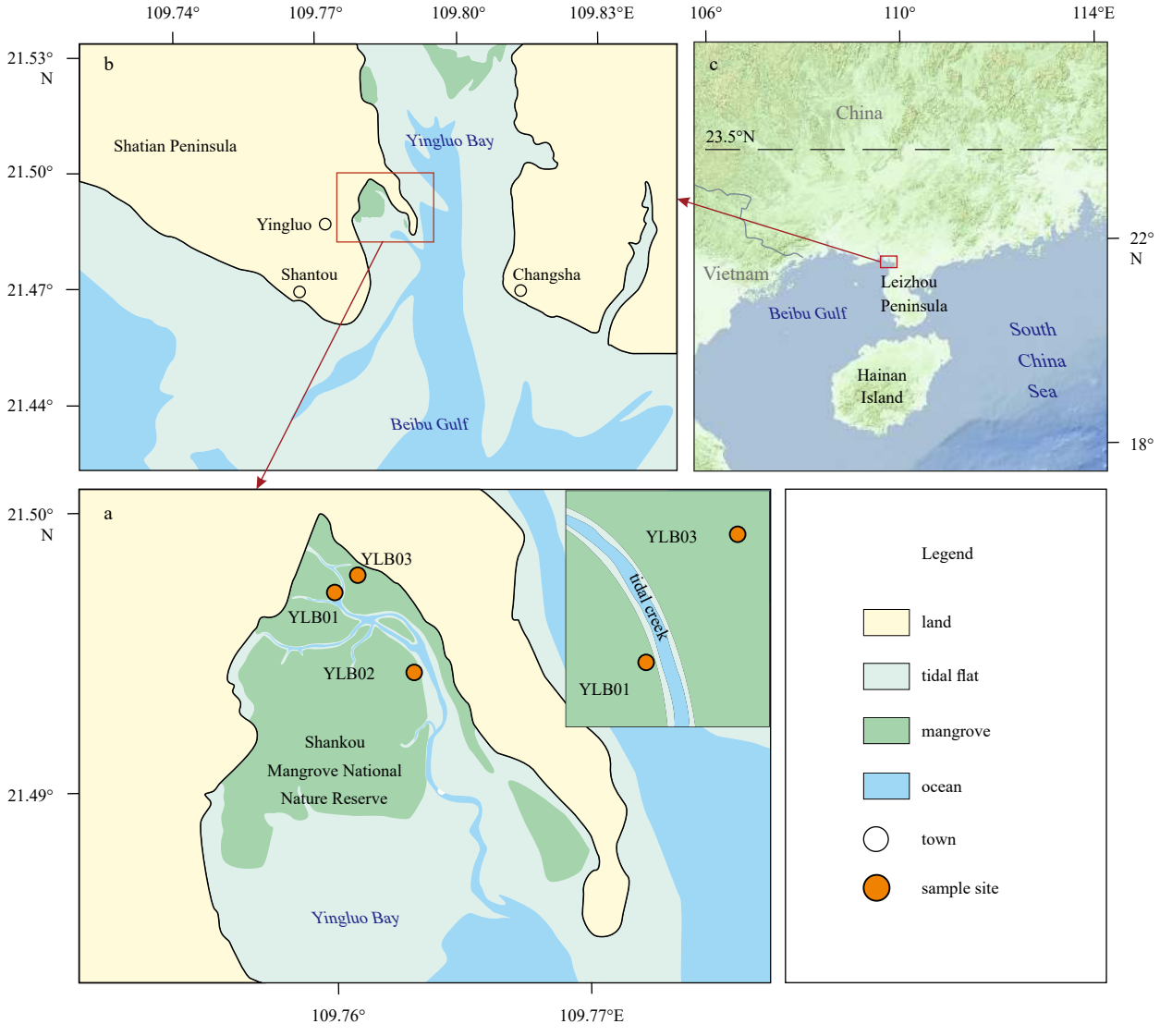

Fig. 1. Locations of sediment cores of YLB01, YLB02, and YLB03 in the Yingluo Bay (a), northern Beibu Gulf (b), China (c).

37.4°C and –0.8°C, respectively. The average annual rainfall is 1 815 mm, 80%–85% of which falls during the summer rainy season (April to September). The region experiences an irregular diurnal tide with a mean tidal range of 2.5 m (Meng and Zhang, 2014). The features of the seawater, which are only affected by monsoonal rainfall, are relatively stable, with a mean temperature of 23.5°C, salinity of 20–23, and pH of 7.6–7.8 (Fan et al., 2005).

In this study, three sediment cores (YLB01, YLB02 and YLB03) were collected from the SMNNR during May 2011 using PVC tubes with a length and internal diameter of 120 cm and 10 cm, respectively (Fig. 1a). The detailed properties of these cores are provided in Table 1. Cores were collected equidistantly from trees to minimize the effects of mangrove roots and crab burrows (Alongi et al., 2005). The sediments collected in the tubes were extruded stepwise using a manual piston and cut into columniform subsamples with a thickness of 2 cm. All subsamples were then stored in tinfoil and polyethylene box at 4°C for further laboratory analysis.

Table 1. Basic information of mangrove sediment cores in the Yingluo Bay, tropical China

Site	Latitude	Longitude	Length /cm	Position in mangrove	Geomorphic setting	Mangrove species
YLB01	21°29′49″N	109°45′36″E	66	interior	upper tidal flat near the tidal creek	*Rhizophora stylosa, Kandelia candel*
YLB02	21°29′39″N	109°45′48″E	88	fringe	middle tidal flat near the trunk of the tidal creek	*Kandelia candel, Aegiceras corniculatum*
YLB03	21°29′53″N	109°45′38″E	50	interior	upper tidal flat near the land	*Bruguiera gymnorrhiza, Rhizophora stylosa*

2.2 *^{210}Pb activity analysis*

^{210}Pb activity was determined by analyzing the radioactivity of the decay product ^{210}Po at the Qingdao Institute of Marine Geology, assuming that both were at equilibrium (Guo et al., 2007). The Po was extracted, purified, and self-plated onto Ag disks. ^{209}Po was used as a yield monitor and tracer in quantification. Samples were counted by computerized multi-channel α spectrometry with Au-Si surface barrier detectors. The excess ^{210}Pb ($^{210}Pb_{ex}$) specific activity was determined by subtracting the supported ^{210}Pb ($^{210}Pb_{sup}$) activity, assuming that it was in equilibrium with ^{226}Ra, from the measured total ^{210}Pb ($^{210}Pb_{tot}$) specific activity (Krishnaswamy et al., 1971). The value of ^{137}Cs was below the detection limit as its content in sediment cores from habitats located in the Southern Hemisphere and near the Equator, such as tropical China, is extremely low (Arias-Ortiz et al., 2018).

2.3 *Bulk properties analysis*

Macroscopic, thick, living roots were removed from sediments before analysis, while fine roots were retained to maintain the original sedimentary structure and consistency (Smoak et al., 2013). This approach is consistent with the method followed in other studies on the OCAR and standing stock in mangrove sediments (Donato et al., 2011; Breithaupt et al., 2012).

The grain size distributions were measured using a Malvern Mastersizer 2000 laser particle analyzer (Malvern, UK) at a measurement range of 0.02–2 000 μm and size resolution of 0.01Φ after removing the organic matter (OM) and carbonate fractions by adding 15 mL 3% H_2O_2 and 5 mL 10% HCl, respectively. All sample preparation and measurement processes were conducted at the Key Laboratory of Marine Geology and Metallogeny, First Institute of Oceanography, Ministry of Natural Resources.

The freeze-dried sediment samples were treated with 1 mol/L of HCl for 24 h at room temperature (25°C) to remove the inorganic carbon and then rinsed with ultra-pure water several times until neutral (pH=7) was achieved, and left to dry at 50°C for 72 h. Approximately 30–40 mg of homogenized dry sediments were carefully placed in tin capsules and crimp-sealed for analysis. The stable organic carbon isotope (δ^{13}C), total organic carbon (TOC), and total nitrogen (TN) contents were determined using a Delta Plus XP mass spectrometer (Thermo Scientific, Germany) coupled with an elemental analyzer (Flash EA 1112, CE Instruments, UK) in the continuous flow mode at the Stable Isotope Laboratory of the College of Resources and Environmental Sciences, China Agricultural University (Beijing). The results are reported in standard delta notation (δ) using permitted units (‰):

$$\delta\,(‰) = (R_{\text{sample}} - R_{\text{standard}})/R_{\text{standard}} \times 1\,000, \quad (1)$$

where δ represents the stable isotope value of organic carbon, and R is the ^{13}C/^{12}C ratio. The Vienna PeeDee Belemnite (VPDB) was used as the reference standard for carbon. The analytical precisions of the ^{13}C, TOC, and TN contents were ±0.2‰, ± 0.02%, and ± 0.005% (according to weight), respectively. The C/N was calculated as the atomic ratio of the TOC to TN.

2.4 *Organic carbon accumulation rate*

Dry bulk density (DBD, g/cm^3) was determined as the dry sediment weight (the sediment was dried at 105°C for over 72 h) divided by the initial volume, using pre-weighed stainless steel specimen cups (Matos et al., 2020). And then, the OCAR (g/(m^2·a), according to carbon) can be calculated by multiplying the sedimentary rates (SR, cm/a) by the sediment dry bulk density (DBD) and OC (percentage) content, as follows (Sanders et al., 2010; Hapsari et al., 2017):

$$\text{OCAR} = \text{SR} \times \text{DBD} \times \text{OC} \times 100, \quad (2)$$

where the SR was determined from the ^{210}Pb chronology (see Section 3.1).

2.5 *Endmember mixing model*

Endmember mixture models can be used to quantitatively calculate the relative contribution of different potential OC sources to a sample (Dittmar et al., 2001; Gonneea et al., 2004). The model based on the δ^{13}C and C/N has been widely used to identify the sources of OM in the sediments and/or suspended solids of different ecosystems such as rivers, lakes, coasts, and the deep sea (Gonneea et al., 2004; Meng et al., 2017; Dong et al., 2020; Zhang et al., 2021). In general, the potential endmembers of OC sources in mangrove sediments mainly include terrestrial matter, mangrove production, and marine phytoplankton (see Section 4.1.1; Xia et al., 2015; Meng et al., 2016, 2017). The formulas of the ternary mixing model based on δ^{13}C and C/N are as follows:

$$\delta^{13}C_{\text{sample}} = (f_A \times \delta^{13}C_A) + (f_B \times \delta^{13}C_B) + (f_M \times \delta^{13}C_M), \quad (3)$$

$$C/N_{sample} = (f_A \times C/N_A) + (f_B \times C/N_B) + (f_M \times C/N_M), \quad (4)$$

$$f_A + f_B + f_M = 1, \quad (5)$$

where A, B, and M are the potential OM end-members and f represents the contributory percentage of each endmember. The $\delta^{13}C$ and C/N values of the endmembers will be discussed in Section 4.1.1. Notably, when the OC in a sample is a mixture of two sources, it should be explained using a binary mixing model with $\delta^{13}C$.

$$\delta^{13}C_{sample} = (f_A \times \delta^{13}C_A) + (f_B \times \delta^{13}C_B), \quad (6)$$

$$f_A + f_B = 1. \quad (7)$$

2.6 *Statistics and visualization*

Pearson correlation analysis and two-tailed significance tests were conducted to determine the correlation between the different parameters. Correlations were considered significant at $p<0.05$. Data analyses were conducted using SPSS 22.0 (SPSS, USA) for Windows, and the "±" symbol represents the standard deviation. The maps and diagrams were mainly produced using Surfer 15, Grapher 13 (Golden Software, USA), and CorelDRAW 2018 (Corel, Canada).

3 Results

3.1 *^{210}Pb chronology*

The plots of the ^{210}Pb chronology for the three cores are shown in Fig. 2. The $^{210}Pb_{tot}$ remained almost constant below depths of 49 cm, 49 cm, and 39 cm at YLB01, YLB02, and YLB03, respectively (Figs 2a, f and k). Thus, these values can be used as the $^{210}Pb_{sup}$ according to the variations in $^{210}Pb_{tot}$ with depth. The calculated $^{210}Pb_{ex}$ at YLB01, YLB02, and YLB03 were (45.48±33.84) Bq/kg, (21.41±19.32) Bq/kg, and (21.59±17.56) Bq/kg, respectively. The imperfect $^{210}Pb_{ex}$ profiles prepared to establish the age model must be corrected by sediment compaction (Robbins and Edgington, 1975), due to the various DBD at different depths (Figs 2b, g, and l). The cumulative mass depth for each sediment core was determined by DBD and the thickness of each interval (Sanchez-Cabeza and Ruiz-Fernández, 2012).

Three models are widely used to establish the ^{210}Pb age model, i.e., the constant flux-constant sedimentation (CF–CS), constant rate of supply (CRS), and constant initial concentration (CIC) models. The CIC model requires a monotonic down-core decrease in the $^{210}Pb_{ex}$ specific activity to avoid age reversals, which is rarely used for most vegetated coastal sediments due to its restrictive hypothesis (Sanchez-Cabeza and Ruiz-Fernández, 2012; Arias-Ortiz et al., 2018). In this case, the calculation of mean accumulation rates alone using the CF–CS model may be more reasonable (Krishnaswamy et al., 1971; Arias-Ortiz et al., 2018). However, the CRS model has been widely applied and validated in estuarine environments and vegetated coastal ecosystems (Breithaupt et al., 2014, 2020) as it is less restricted by issues associated with non-monotonic features in the ^{210}Pb record and is relatively insensitive to mixing (Appleby and Oldfield, 1992).

The CRS model was preferentially used to study the ^{210}Pb chronological framework in this study. The mass accumulation rates (MARs) were 0.34 g/(cm^2·a) (0.12–0.79 g/(cm^2·a)), 0.56 g/(cm^2·a) (0.48–0.87 g/(cm^2·a)), and 0.47 g/(cm^2·a) (0.22–0.73 g/(cm^2·a)) in YLB01, YLB02, and YLB03, respectively (Figs 2c, h, and m). The average MARs based on the CF–CS model were 0.43 g/(cm^2·a), 0.56 g/(cm^2·a), and 0.47 g/(cm^2·a) in YLB01, YLB02, and YLB03, respectively, according to the ln($^{210}Pb_{ex}$) and mass depth after eliminating the impacts of the surface mixing layer (Figs 2d, i, and n). The reliability of the CRS model was demonstrated by the similar ^{210}Pb chronological results calculated using the CF–CS model (Figs 2e, j, and o). The SR in each layer was obtained by the MAR and DBD values (Sanchez-Cabeza and Ruiz-Fernández, 2012), and its mean values in the three cores were close to those reported in previous studies on the Guangxi coasts (Xia et al., 2015; Meng et al., 2016). The ^{210}Pb geochronology was dated up to depths of 49 cm, 49 cm, and 39 cm in YLB01, YLB02, and YLB03, corresponding to the years of 1890 AD, 1897 AD, and 1887 AD, respectively. Therefore, the sedimentary history since 1900 in the study area can be reconstructed.

3.2 *Bulk properties*

Cores YLB01 and YLB03 were both obtained in the mangrove interior, while Core YLB02 was obtained in the mangrove fringe of the SMNNR (Fig. 1a). Specifically, YLB01 was obtained near a small branch of the tidal creek, while YLB03 was obtained closer to land, and YLB02 was obtained near the trunk of the tidal creek (Table 1). The bulk properties of these cores are shown in Fig. 3, including the grain size, TOC, TN, C/N, and $\delta^{13}C$.

3.2.1 *Mangrove interior cores (YLB01 and YLB03)*

The proportions of sand, silt, and clay in the sediment of Core YLB01 were 17.3%, 61.8%, and 20.9%, respectively. The mean grain size (M_z) varied from 5.39Φ to 6.39Φ, with an average of (6.23±0.46)Φ. The TOC and TN contents were (2.03±0.37)% and (0.12±0.03)%, respectively, and had increased since 1900. The C/N value ranged between 11.9 and 35.5, with a mean of 20.1±4.41. The average $\delta^{13}C$ value was (–27.3±0.6)‰, ranging from –28.1‰ to –25.4‰, and had gradually decreased since 1900.

The sand, silt, and clay contents in the sediment of Core YLB03 were 42.9%, 43.2%, and 13.9%, respectively. The M_z varied from 3.74Φ to 6.25Φ, with an average of (4.76±0.54)Φ. The C/N value ranged between 12.3 and 28.3, with a mean of 19.2±3.68. Similar to Core YLB01, the TOC and TN contents had increased trend since 1900, while $\delta^{13}C$ followed an opposite trend. The TOC and TN contents were (1.14±0.42)% and (0.07±0.02)%, respectively, while the average $\delta^{13}C$ value was (–27.3±0.6)‰, ranging from –29.2‰ to –26.9 ‰.

3.2.2 *Mangrove fringe core (YLB02)*

The proportions of sand, silt, and clay in the sediment of core YLB02 were 30.1%, 51.4%, and 18.5%, respectively. The M_z varied from 4.06Φ to 7.29Φ, with an average of (5.65±1.02)Φ. The TOC and TN contents were (1.29±0.63)% and (0.08±0.04)%, respectively. The C/N value ranged between 14.4 and 23.5, with a mean value of 19.0±2.05. The average $\delta^{13}C$ value was (–27.9±0.6)‰, ranging from –28.8‰ to –26.6‰. This core can be divided into two sections bounded by the 1940s according to the variations in the bulk properties over time. Before the 1940s, the sediment composition, M_z, TOC, TN, and $\delta^{13}C$ were relatively stable, while these values were very different after the 1940s since the abrupt change in the 1940s. The overall trends of the TOC and TN contents were contrary to those of YLB01 and YLB03, while the total trend of the $\delta^{13}C$ value was consistent with that of the other cores.

3.3 *Organic carbon accumulation rate*

The OCAR value in the Yingluo Bay since 1900, which were calculated using Eq. (2), are shown in Fig. 4. In Core YLB01, the OCAR varied from 12.7 g/(m^2·a) to 216.12 g/(m^2·a) (according to carbon), with an average of (91.7±47.7) g/(m^2·a) (according to carbon) (Fig. 4a). The average OCAR value in Core YLB02 was

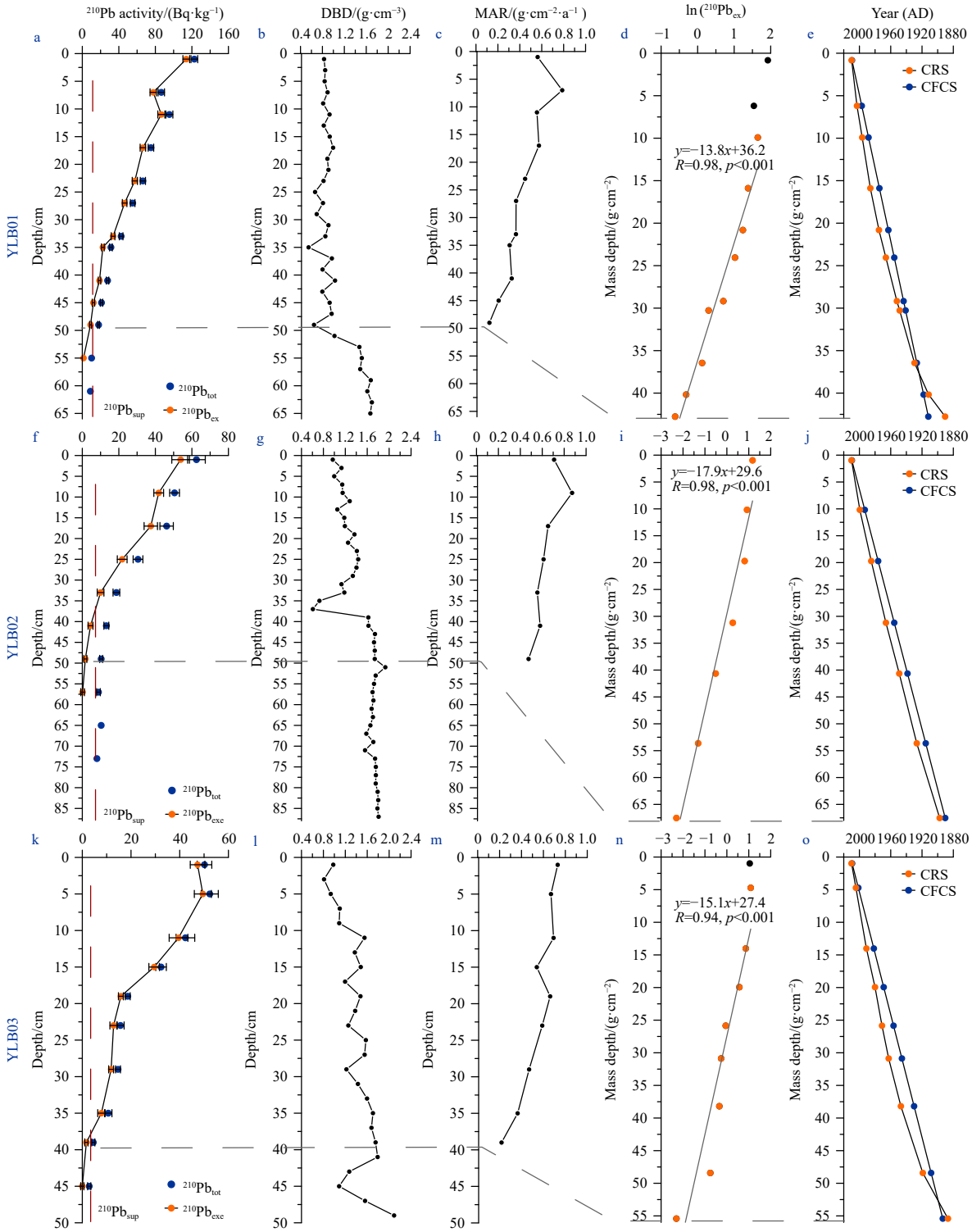

Fig. 2. Vertical profiles of ^{210}Pb activity, dry bulk density (DBD), and mass accumulation rate (MAR) vs. depth, and ln(^{210}Pb$_{ex}$) and ages vs. mass depth in sediment cores of YLB01 (a–e), YLB02 (f–j), and YLB03 (k–o).

(76.8±32.8) g/(m²·a) (according to carbon), which ranged from 4.5 g/(m²·a) (according to carbon) to 135.8 g/(m²·a) (according to carbon) (Fig. 4b). In Core YLB03, the OCAR ranged between 7.9 g/(m²·a) (according to carbon) and 135.8 g/(m²·a) (according to carbon), with a mean value of (65.6±36.3) g/(m²·a) (according to carbon) (Fig. 4c). In the mangrove interior (i.e., Cores YLB01 and YLB03), the OCAR had increased since 1900. In contrast, the changes in the OCAR of the mangrove fringe (i.e., Core YLB02) decreased with oscillations. The most notable change occurred in the 1940s, which agreed with the variations in the other parameters, such as the grain size, TOC, TN, and δ^{13}C (Fig. 3). Before the 1940s, the OCAR in the mangrove fringe was obviously higher than that in the mangrove interior with a collectively increasing trend with time; however, after the 1940s, the change in the

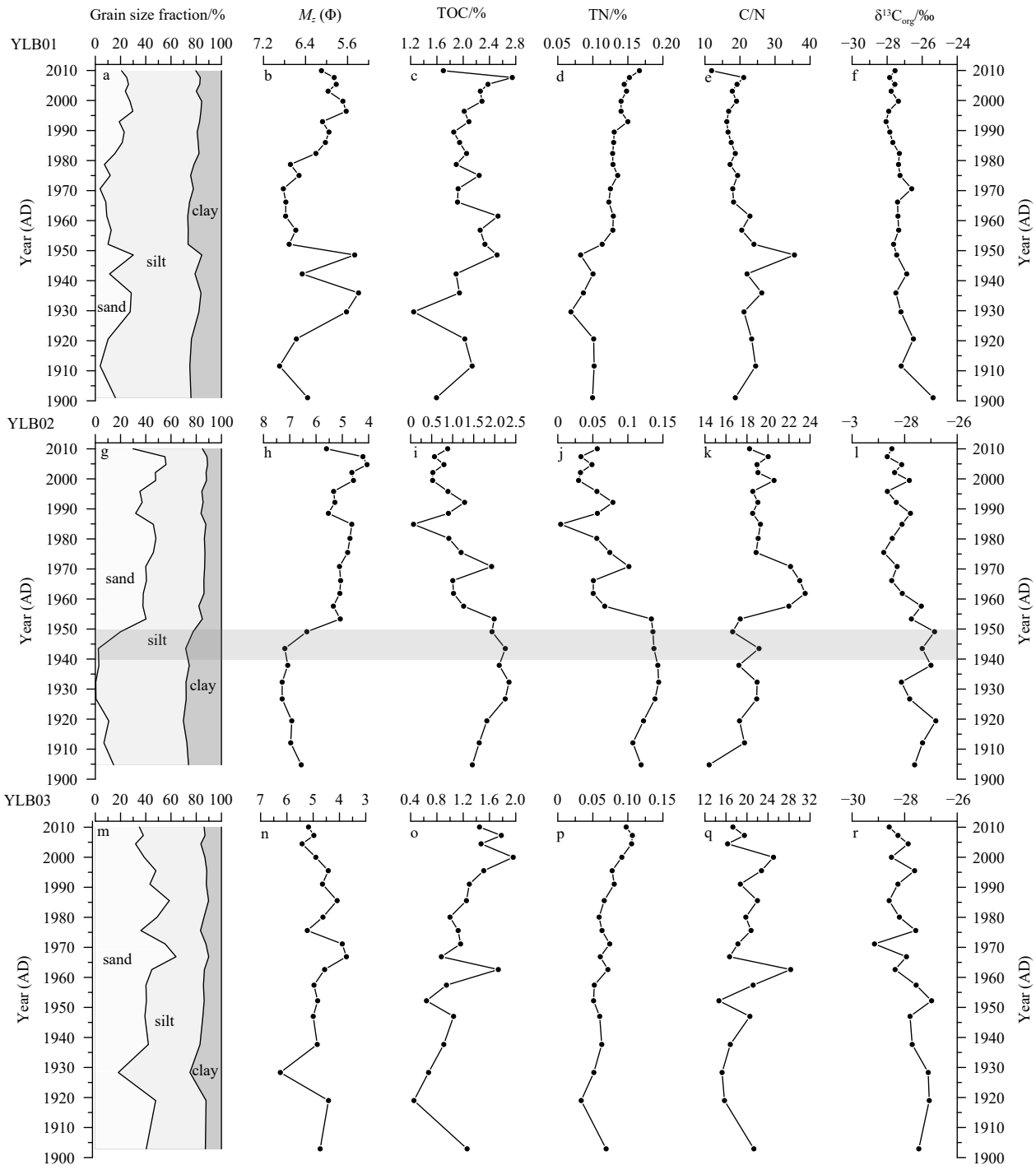

Fig. 3. Variations in the grain size fraction, mean grain size (M_z), total organic carbon (TOC) and total nitrogen contents (TN), atomic C/N ratio, and stable organic carbon isotopes ($\delta^{13}C_{org}$) in sediment cores of YLB01 (a–f), YLB02 (g–l), and YLB03 (m–r) since 1900.

OCAR of the mangrove fringe constantly oscillated and was lower than that of the mangrove interior (Fig. 4).

4 Discussion

4.1 *Organic carbon sources*

4.1.1 *Potential sources of organic carbon and their end-member values*

The OC stored in mangrove sediments is the refractory fraction remaining after decomposition and originates from autochthonous and allochthonous inputs. The autochthonous inputs include mangrove (i.e., mangrove roots and leaf litters) and microbial (e.g., bacteria) production, while the allochthonous inputs include terrestrial matter and marine phytoplankton (Bouillon et al., 2004; Sasmito et al., 2020). However, microbes alone contribute less than 1% of the OC in mangrove sediments (Bouillon et al., 2004). Therefore, terrestrial matter, mangrove production, and marine phytoplankton can be considered as the potential endmembers of the sedimentary OC sources in this study.

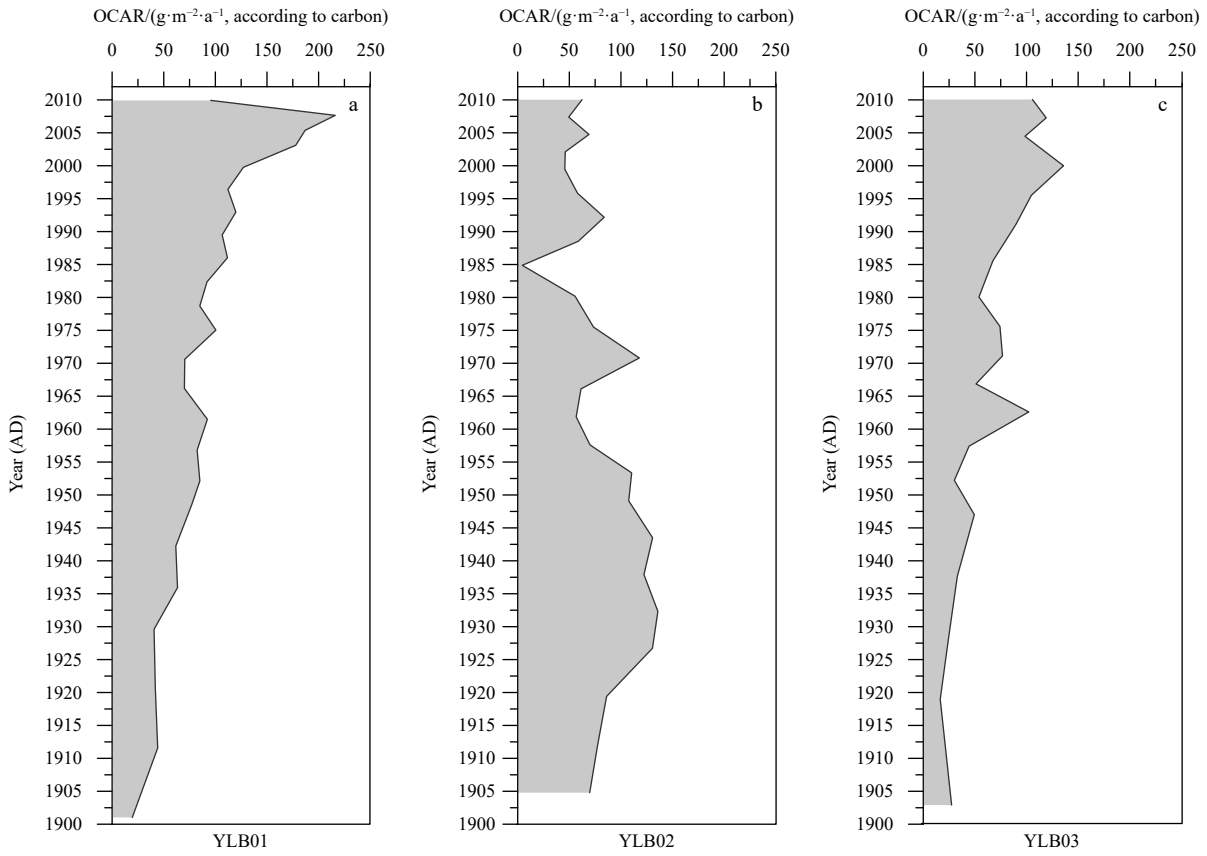

Fig. 4. Variations in the organic carbon accumulation rate (OCAR) in sediment cores of YLB01 (a), YLB02 (b), and YLB03 (c) since 1900.

Notably, previous studies in the Yingluo Bay and Qinzhou Bay, South China, show that the contribution of marine input to sedimentary OC is estimated to be <5% (Xia et al., 2015; Meng et al., 2016), which may be caused by the lower primary production and stronger ebb-tidal current with the irregular diurnal tide (Meng and Zhang, 2014).

The average $\delta^{13}C$ and C/N values of the leaves of different mangrove species (n=24) collected along the Guangxi coasts are (−28.7±0.8)‰ and (36.4±7.3) (Xia et al., 2015; Meng et al., 2016), respectively, which are consistent with those from the Hainan Island, tropical China (Herbeck et al., 2011). Although mangrove roots and leaf litter are both important OC sources in mangrove sediments, the $\delta^{13}C$ and C/N values of roots are generally within the range of, or overlap, those of leaf litter (Kusumaningtyas et al., 2019; Sasmito et al., 2020). Therefore, the $\delta^{13}C$ and C/N values of Guangxi mangrove leaves can be regarded as the endmember values of mangrove production. The terrestrial and marine endmembers were represented by the riverine sediments from the rivers flowing into the northern Beibu Gulf ($\delta^{13}C$=(−24.3±0.6)‰; C/N=12.6±1.9) and phytoplankton in the northern South China Sea ($\delta^{13}C$=(−16.1±0.8)‰; C/N=(6.5 ± 0.7); Xue et al., 2009; Meng et al., 2016, 2017).

4.1.2 *Sources of organic carbon in mangrove sediments*

The three potential endmembers exhibit a clear separation in the $\delta^{13}C$ vs. C/N scatter plot (Fig. 5), which provided the basis for identifying the OC sources. Most samples of this study were located in the area connecting the mangrove leaves and river sediments, indicating that the OC of the samples was a mixture of only these two endmembers. This result further proved that the contribution of OC from marine phytoplankton could be neglected. Previous studies reported that $\delta^{13}C$ is a more credible tracer for calculating the contributions of OC in sediments, par-

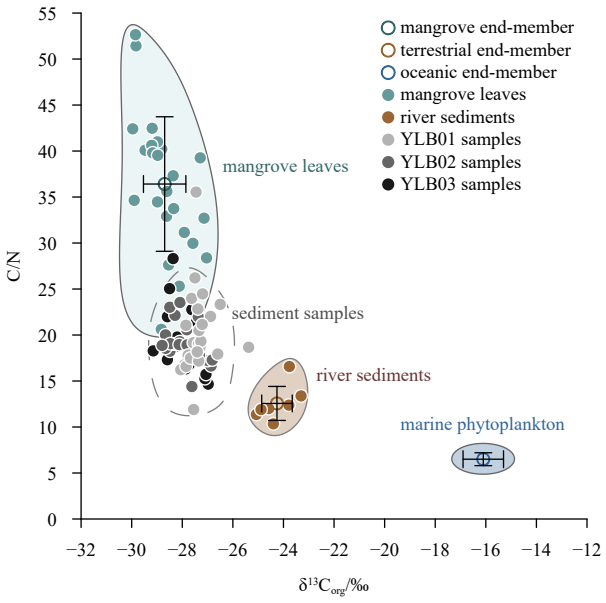

Fig. 5. Scatter diagram of $\delta^{13}C_{org}$ vs. C/N for identifying the organic carbon sources in the three sediment cores. The endmember values are from Xue et al. (2009), Xia et al. (2015), and Meng et al. (2016).

ticularly in sediments with a few OC content (Gonneea et al., 2004), while C/N may be more likely altered by early diagenesis and degradation (Lamb et al., 2006; Xia et al., 2021). Therefore, the contribution of mangrove-derived OC (CMOC) and contribution of terrigenous OC (CTOC) in mangrove sediments can be calculated using a binary mixing model based on the $\delta^{13}C$ value.

The average CMOC and CTOC were (68.5±12.7)% (25.2%–85.7%) and (31.5±12.7)% (14.3%–74.8%) in Core YLB01 (Fig. 6a), respectively. The average CMOC was higher in Core YLB02 (Fig. 6b), with a mean value of (81.6±13.8)% (52.8%–100%), whereas the CTOC was only (18.4±13.8)% (0–47.2%). The average CMOC and CTOC in Core YLB03 were (82.6±11.7)% (61.2%–100%) and (17.4±11.7)% (0%–38.8%), respectively (Fig. 6c). Overall, the changes in the CMOC in the three cores all increased over time.

4.2 *Tracing mangrove development by the contribution of mangrove-derived organic carbon*

The application of CMOC has successfully reconstructed the histories of mangrove development with different time scales in different regions of the tropics, e.g., western coast of peninsular India (Caratini et al., 1994), Flamenco Lagoon in Puerto Rico (França et al., 2014), Maowei Sea in tropical China (Meng et al., 2016), and the Amazon Estuary of northern Brazil (Cohen et al., 2016). Therefore, the CMOC is an effective proxy for recovering regional mangrove development (Xia et al., 2021). The CMOC of the three cores from the Yingluo Bay had all increased since 1900 based on the linear regression (Fig. 6; Figs 7a–c), indicating that mangrove forests have flourished in this region since 1900. The mangrove pollen (MP) content is also one of the simplest and most effective proxies for tracing mangrove evaluation (Gonneea et al., 2004; Ellison, 2008; Li et al., 2008). The tendency of the MP content in the Yingluo Bay since 1900 (Xia et al., 2015) was consistent with that of CMOC (Figs 7a–d), further demonstrating the gradual mangrove flourishment in the Yingluo Bay since 1900.

4.3 *Factors controlling the spatiotemporal variations in the organic carbon accumulation rate*

The accumulation of OC in mangrove sedimentary systems is affected by numerous processes, including the supplies of OC from several sources, settlement of particulate OC in tidal water, re-suspension of sedimentary OC, seaward migration and final export of OC by the ebb-tidal current, and the post-depositional decomposition of OC (Kristensen et al., 2008). In brief, mangrove OC accumulation is the ultimate outcome of the balance between OC production and decomposition under the effects of sedimentary processes, and this balance can be affected and altered by several factors that can vary and be site-specific (Hapsari et al., 2017). In this study, the potential factors influencing the OCAR in the Yingluo Bay mainly contained mangrove development, regional climate, hydrological condition, and sea-level.

4.3.1 *Mangrove development and climate*

The OC supply and accumulation can be affected by man-

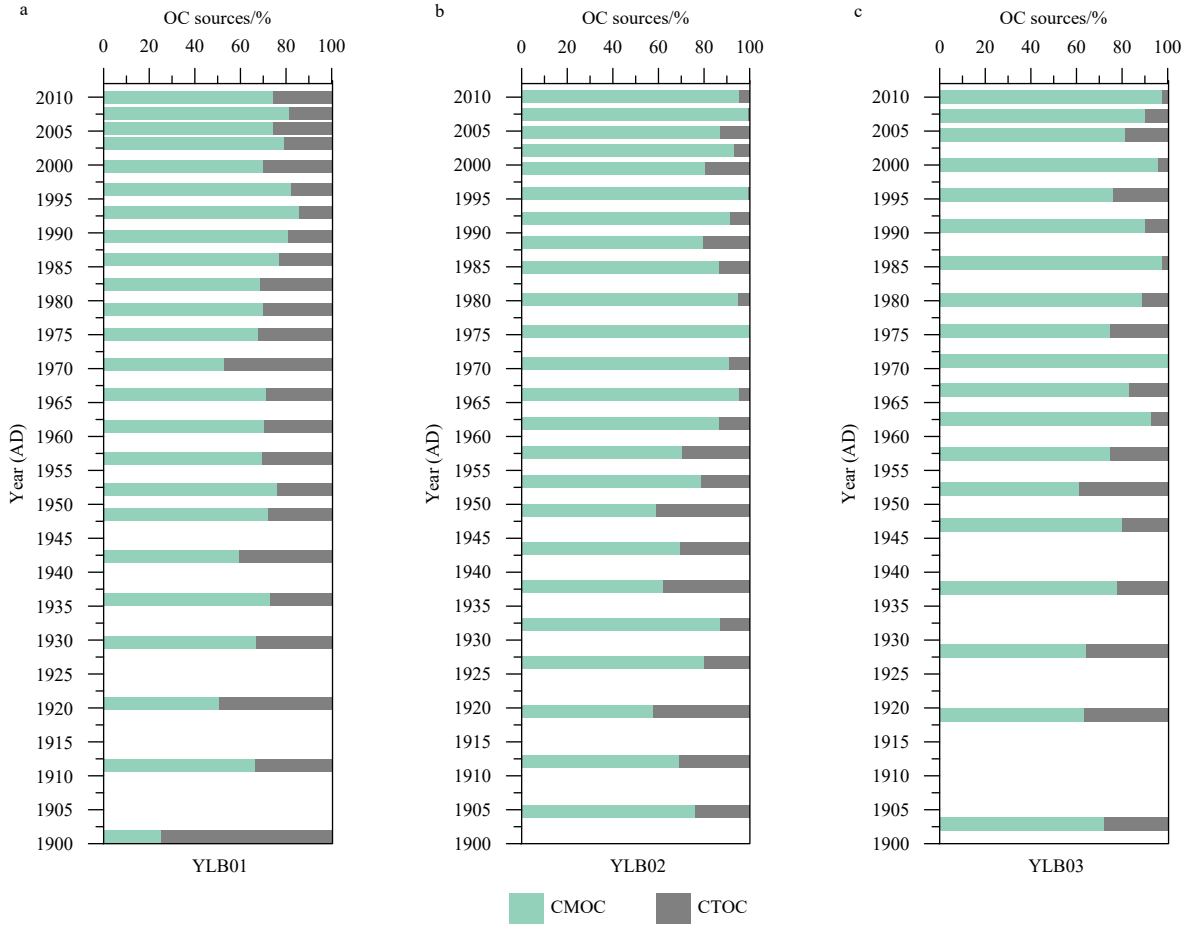

Fig. 6. Variations in the contributions of mangrove-derived organic carbon (CMOC) and terrestrial organic carbon (CTOC) in sediment cores of YLB01 (a), YLB02 (b), and YLB03 (c) since 1900.

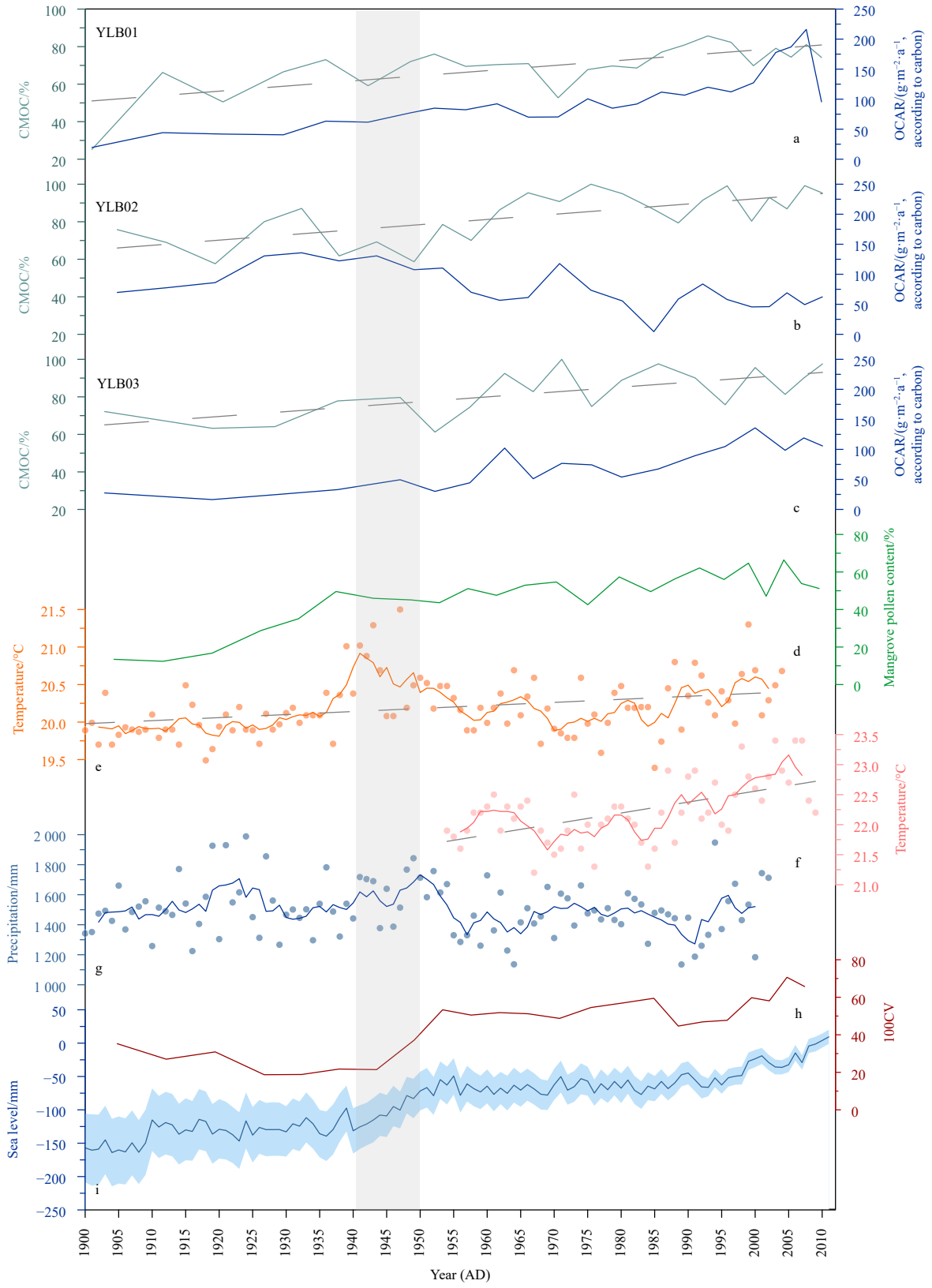

Fig. 7. Variations and comparison of the organic carbon accumulation rate (OCAR) and contribution of mangrove derived organic carbon (CMOC) in the sediment cores (a–c), mangrove pollen content (Xia et al., 2015) (d), annual average air temperature and average rainfall of Guangxi (e and g) and average air temperature of Beihai City (f) (Huang et al., 2007), coefficient of grain size variation (100CV) of mangrove fringe (YLB02) (h), and sea level changes in the study region (i) (Frederikse, et al., 2020) since 1900. The blue shaded area represents the range of sea-level change. The solid lines in e, f, and g represent the 5 a moving averages of the original data sets. The grey dashed lines are linear regression of the corresponding data sets.

grove development, which was traced by CMOC, as mangroves were the most important OC contributor ((77.2±14.4)%) in the Yingluo Bay. The influences of mangrove development on the variations in OCAR were determined by calculating the correlation coefficients between the OCAR and CMOC (Figs 8a–c) and assessing the parallel relationships between their changes over time (Figs 7a–c). For Cores YLB01 and YLB03, which were collected from the mangrove interior, the variations in OCAR since 1900 were overall consistent with their corresponding CMOC values (Figs 7a and c), with significant positive correlations of R=0.64 (p<0.01, n=25) and R=0.71 (p<0.01, n=20), respectively (Figs 8a and c). The results indicated that the variations in the OCAR at the interior of mangrove forests were mainly controlled by mangrove development. That is, the increase in the OCAR since 1900 was due to mangrove flourishment.

Climate change and anthropogenic activity are two significant factors controlling the evolution of mangrove forests on the centurial time scale (Xia et al., 2015; Meng et al., 2016; Veettil et al., 2019) and should be considered as the further potential reasons for the variations in OCAR. The SMNNR in the Yingluo Bay is located far away from industrial areas and city centers, and is considered natural, i.e., not influenced by human activity (Xia et al., 2015). To determine if the observed changes in mangrove development were related to regional climatic fluctuations, this study compared the CMOC records in the Cores YLB01 and YLB03 with the annual average air temperature of Beihai since 1953, and the annual average air temperature and rainfall of Guangxi since 1900 (Figs 7e–g) recorded by the Guangxi Climate Center (Huang et al., 2007). The Morlet wavelet analysis results indicated an increasing trend for temperature, accompanied by quasi-biennial oscillations in the temperature variations, while precipitation exhibited a decreasing trend with 32 a and quasi-biennial oscillations (Huang et al., 2007). The growing trends of CMOC and OCAR were consistent with those of temperature (Fig. 7e) instead of the precipitation (Fig. 7g), particularly for OCAR and temperature since 1953 (Fig. 7f). Generally, a gradual rise in temperature will promote mangrove growth and result in the expansion of mangroves towards higher latitudes (Osland et al., 2017). Therefore, climate change characterized by rising temperatures was the key factor causing mangrove flourishment and the associated increase in the OCAR of the mangrove interior area, which was consistent with previous findings in the Yingluo Bay (Xia et al., 2015).

The variations in OCAR were not parallel with their corresponding CMOC in Core YLB02, which was collected from the mangrove fringe (Fig. 7b), with a poor correlation (R=0.16, p>0.1, n=25; Fig. 8b), meaning that there were other factors controlled the OCAR variations since 1900.

4.3.2 *Hydrological condition and sea level*

The coefficient of the grain size variation (CV), which is defined as the ratio of the standard deviation (i.e., sorting coefficient) and M_z, can be used to evaluate the hydrodynamic intensity (Yang et al., 2014). For the sake of clear expression, this study enlarge it 100 times and express it as 100 CV. At the sites located in the mangrove interior (YLB01 and YLB03), there was no correlation between OCAR and 100CV (Figs 8d and f), with R values of 0.11 (p>0.5, n=25) and 0.05 (p>0.5, n=20), respectively, while the OCAR were significantly and positively correlated with CMOC (Figs 8a and c). These results further indicate that the variations of OCAR in the mangrove interior were primarily affected by local mangrove development instead of hydrodynamic conditions.

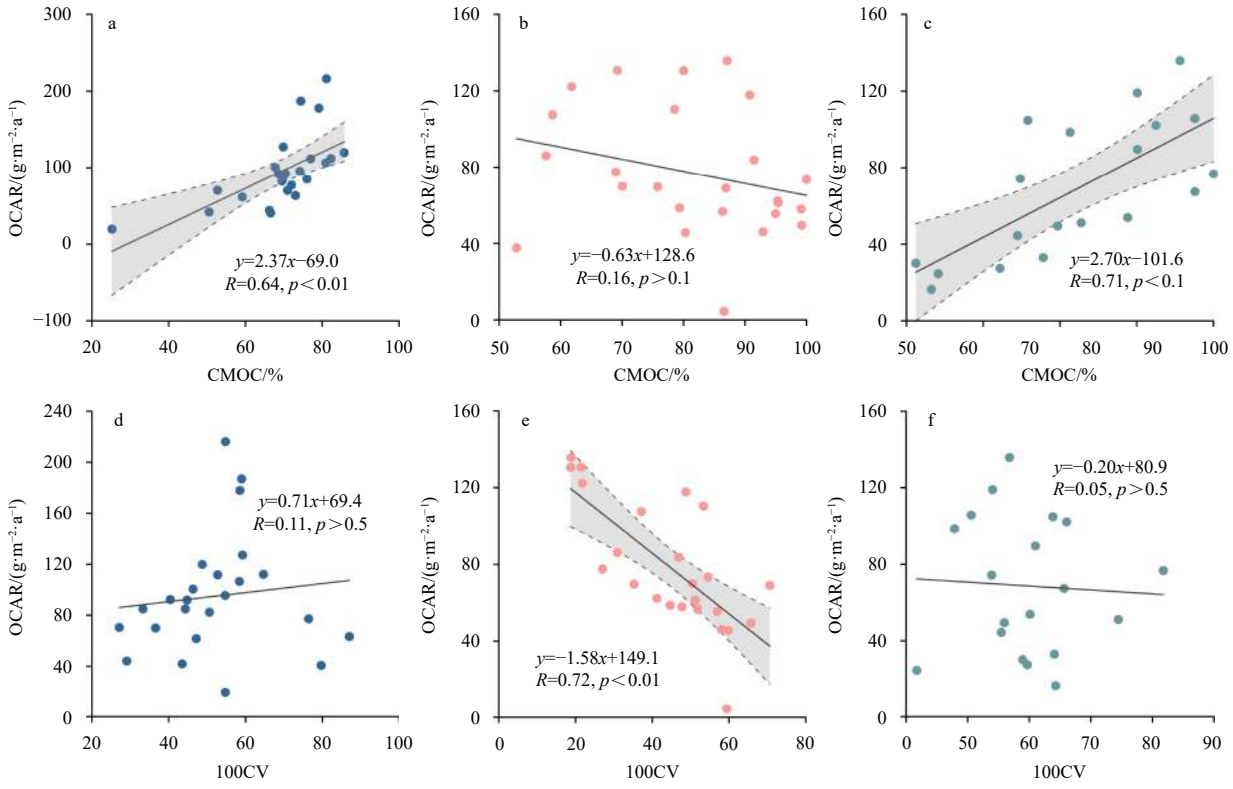

Fig. 8. Bivariate plots of the organic carbon accumulation rate (OCAR) vs. the contribution of mangrove-derived organic carbon (CMOC) and coefficient of grain size variation (100CV) in sediment cores of YLB01 (a and d), YLB02 (b and e), and YLB03 (c and f). The dashed lines and shaded areas represent the 95% confidence intervals.

However, for the site in mangrove fringe (YLB02), the variation tendency of OCAR was in contrast with its corresponding 100CV (Figs 7b and h), with a significant negative correlation (R=0.72, p<0.01, n=25) (Fig. 8e), indicating that the hydrodynamic condition, especially the to-and-fro tide, was the main factor affecting the OCAR in the mangrove fringe since 1900.

Mangroves, located on intertidal sediments with a gentle slope, are very sensitive to sea-level changes (Woodroffe et al., 2016). A sea-level rise will strengthen the tidal (wave) energy under the background of climatic warming, which can accelerate the oxidative decomposition of OM and reduce its burial efficiency in sediments with the increasing sediment grain size (Breithaupt et al., 2012; Smoak et al., 2013; Yang et al., 2014; Arias-Ortiz et al., 2018; Veettil et al., 2019). In the SMNNR, which is free from human influence, the variations in the hydrodynamic conditions were likely to be induced by sea-level changes, which was a further factor impacting the OCAR. In this study region, the sea-level has increased since 1900 (Fig. 7i) in accordance with the global sea-level rise (Frederikse et al., 2020). Before the 1940s, the sea-level exhibited a gradually increasing trend (0.6 mm/a), corresponding to a lower 100CV and higher OCAR value in mangrove fringe (Figs 7b and h). After the 1940s, the sea level increased obviously, which corresponds to the increasing 100CV and decreasing OCAR in mangrove fringe. In particular, the sea level abruptly increased by approximately 5.5 mm/a during 1940–1955, and meanwhile, the sediment composition coarsened (Fig. 3g), 100CV increased (Fig. 7h), and OCAR decreased (Fig. 7b) remarkably. Therefore, the strengthening hydrodynamic conditions, induced by sea level rise, still limited the OC accumulation, even if mangrove degeneration did not occur and maintained normal OM production (Fig. 7b). Additionally, the intensity and frequency of extreme weather and climate events have increased on a global scale (Bellprat et al., 2019), e.g., increasing rainstorms in South China since 1960 (Chi et al., 2016), which would also strengthen hydrodynamic conditions, leading to sediment resuspension and promoting OM decomposition (Breithaupt et al., 2012; Smoak et al., 2013; Kusumaningtyas et al., 2019). This may be another potential reason for the low OCAR in the mangrove fringe after the 1940s.

The hydrological conditions and sea level rise should also be responsible for the spatial variability of OCAR between the mangrove interior (YLB01 and YLB03) and fringe (YLB02). The duration of seawater inundation plays an important role in controlling the site-specific OCAR. Longer duration of seawater inundation favors additional capture of OC from both mangrove plants and allochthonous sources and restricts the OC decay induced by aerobic respiration, which are critical mechanisms causing decreases in the OCAR from the seaward to landward fringes of mangroves (Sanders et al., 2010; Breithaupt et al., 2020). Specifically, YLB03 was closer to land in the mangrove interior, while YLB01 was located near a small branch of the tidal creek in the mangrove interior, and YLB02 was located near the trunk of the tidal creek in the mangrove fringe (Table 1). Therefore, the OCAR decreased from YLB02 to YLB01 and YLB03, i.e., from the sea to the land, before the 1940s (Fig. 4). However, the strengthened hydrodynamic conditions mentioned above broke this pattern after the 1940s, resulting in a relatively low OCAR in YLB02 (mangrove fringe) during this period, while this trend remained at YLB01 and YLB03 (mangrove interior; Fig. 4) and the OCAR increased along with mangrove development, as the strong wave energy will be eliminated by the blocking effect of the dense and complex aerial root systems (e.g., prop roots and pneumatophores) in mangrove forests (Duke et al., 2007).

To sum up, the variations of OCAR over time since 1900 were the ultimate outcome of the balance between OC production induced by mangrove development and OC decomposition caused by hydrodynamic intensity (Fig. 9). Meanwhile, the hydrologic condition (i.e., duration of tidal inundation and tidal current intensity) controlled the spatial change of OCAR (Fig. 9). At present, the research on OCAR of mangrove sediments mostly focuses on its spatial variation. Similar to the findings of this study, a previous study regarding the OCAR in four areas of the Leizhou

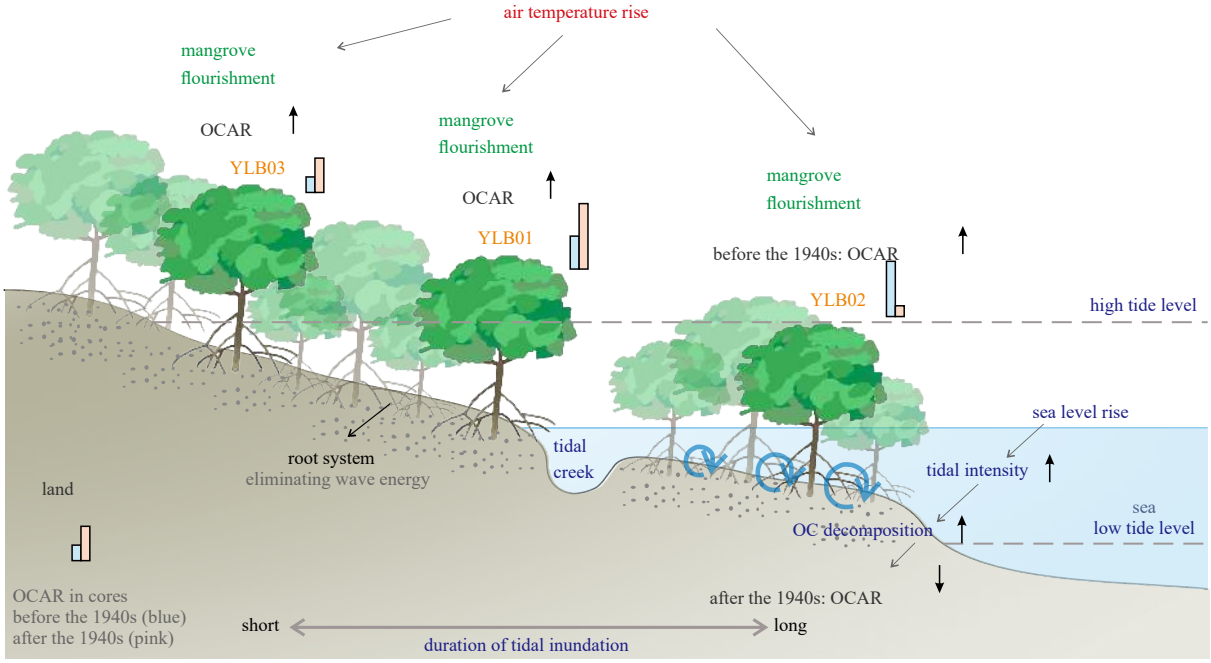

Fig. 9. Conceptual graph of spatiotemporal variations in the organic carbon accumulation rate (OCAR) in mangrove sediments from the Yingluo Bay, tropical China, since 1900.

Peninsula indicate that hydrogeomorphology determined the organic carbon accumulations (Yang et al., 2014). In this study, the guiding ideology in the analysis of spatiotemporal variations in OCAR is the so-called "balance idea", which has been widely used in recent studies regarding OC accumulation in mangrove forests (Kusumaningtyas et al., 2019; Breithaupt et al., 2020; Matos et al., 2020; Sasmito et al., 2020), even in other ecosystems such as tropical peat (Hapsari et al., 2017).

5 Conclusions

This study analyzed the grain size, TOC, TN, C/N, $\delta^{13}C$, and DBD of three sediment cores dated by ^{210}Pb chronology from the mangrove interior (YLB01 and YLB03) and fringe (YLB02) areas of the Yingluo Bay, tropical China. The OC sources were quantitatively identified using an endmember mixing model based on $\delta^{13}C$. The changes in CMOC indicated that mangrove forests had flourished in the Yingluo Bay since 1900. Then this study focused on the spatiotemporal variations in the calculated OCAR of the study area since 1900 and analyzed their influencing factors. The increasing OCAR in the mangrove interior was attributed to mangrove flourishment induced by climate change characterized by the rising temperature. However, in the mangrove fringe, the strengthening hydrodynamic condition under the background of sea level rise was responsible for the decreasing OCAR, particularly after the 1940s. Additionally, the duration of inundation by seawater and hydrodynamic intensity were the primary factors controlling the spatial variability of the OCAR in the studied mangroves.

Acknowledgements

We specially thanks to Tim C. Jennerjahn of the Leibniz Center for Tropical Marine Ecology (ZMT), Bremen, Germany, for the assistance and feedback on our original manuscript. We also thank Guoan Wang from China Agricultural University for the laboratory analysis.

References

Alongi D M. 2014. Carbon cycling and storage in mangrove forests. Annual Review of Marine Science, 6: 195–219, doi: 10.1146/annurev-marine-010213-135020

Alongi D. 2020. Global significance of mangrove blue carbon in climate change mitigation (version 1). Sci, 2(3): 57, doi: 10.3390/sci2030057

Alongi D M, Pfitzner J, Trott L A, et al. 2005. Rapid sediment accumulation and microbial mineralization in forests of the mangrove *Kandelia candel* in the Jiulongjiang Estuary, China. Estuarine, Coastal and Shelf Science, 63(4): 605–618, doi: 10.1016/j.ecss.2005.01.004

Appleby P G, Oldfield F. 1992. Application of ^{210}Pb to sedimentation studies. In: Ivanovich M, Harmon R S, eds. Uranium-Series Disequilibrium. Oxford: Clarendon Press, 31–778

Arias-Ortiz A, Masqué P, Garcia-Orellana J, et al. 2018. Reviews and syntheses: ^{210}Pb-derived sediment and carbon accumulation rates in vegetated coastal ecosystems—setting the record straight. Biogeosciences, 15(22): 6791–6818, doi: 10.5194/bg-15-6791-2018

Bellprat O, Guemas V, Doblas-Reyes F, et al. 2019. Towards reliable extreme weather and climate event attribution. Nature Communications, 10(1): 1732, doi: 10.1038/s41467-019-09729-2

Bouillon S, Moens T, Overmeer I, et al. 2004. Resource utilization patterns of epifauna from mangrove forests with contrasting inputs of local versus imported organic matter. Marine Ecology Progress Series, 278: 77–88, doi: 10.3354/meps278077

Breithaupt J L, Smoak J M, Bianchi T S, et al. 2020. Increasing rates of carbon burial in southwest florida coastal wetlands. Journal of Geophysical Research, 125(2): e2019JG005349

Breithaupt J L, Smoak J M, Smith III T J, et al. 2012. Organic carbon burial rates in mangrove sediments: Strengthening the global budget. Global Biogeochemical Cycles, 26(3): GB3011

Breithaupt J L, Smoak J M, Smith III T J, et al. 2014. Temporal variability of carbon and nutrient burial, sediment accretion, and mass accumulation over the past century in a carbonate platform mangrove forest of the Florida Everglades. Journal of Geophysical Research, 119(10): 2032–2048

Caratini C, Bentaleb I, Fontugne M, et al. 1994. A less humid climate since ca. 3500 yr B.P. from marine cores off Karwar, western India. Palaeogeography, Palaeoclimatology, Palaeoecology, 109(2–4): 371–384

Chi Xiaoxiao, Yin Zhan'e, Wang Xuan, et al. 2016. Spatiotemporal variations of precipitation extremes of China during the past 50 years (1960-2009). Theoretical and Applied Climatology, 124(3): 555–564

Cohen M C L, Lara R J, Cuevas E, et al. 2016. Effects of sea-level rise and climatic changes on mangroves from southwestern littoral of Puerto Rico during the middle and late Holocene. CATENA, 143: 187–200, doi: 10.1016/j.catena.2016.03.041

Cuellar-Martinez T, Ruiz-Fernández A C, Sanchez-Cabeza J A, et al. 2020. Temporal records of organic carbon stocks and burial rates in Mexican blue carbon coastal ecosystems throughout the Anthropocene. Global and Planetary Change, 192: 103215, doi: 10.1016/j.gloplacha.2020.103215

Dittmar T, Lara R J, Kattner G. 2001. River or mangrove? Tracing major organic matter sources in tropical Brazilian coastal waters. Marine Chemistry, 73(3–4): 253–271, doi: 10.1016/S0304-4203(00)00110-9

Donato D C, Kauffman J B, Murdiyarso D, et al. 2011. Mangroves among the most carbon-rich forests in the tropics. Nature Geoscience, 4(5): 293–297, doi: 10.1038/ngeo1123

Dong Yanru, Li Yue, Kong Fanlong, et al. 2020. Source, structural characteristics and ecological indication of dissolved organic matter extracted from sediments in the primary tributaries of the Dagu River. Ecological Indicators, 109: 105776, doi: 10.1016/j.ecolind.2019.105776

Duarte C M. 2017. Reviews and syntheses: hidden forests, the role of vegetated coastal habitats in the ocean carbon budget. Biogeosciences, 14(2): 301–310, doi: 10.5194/bg-14-301-2017

Duarte C M, Middelburg J J, Caraco N. 2005. Major role of marine vegetation on the oceanic carbon cycle. Biogeosciences, 2(1): 1–8, doi: 10.5194/bg-2-1-2005

Duke N C, Meynecke J O, Dittmann S, et al. 2007. A world without mangroves?. Science, 317(5834): 41–42

Ellison J C. 2008. Long-term retrospection on mangrove development using sediment cores and pollen analysis: a review. Aquatic Botany, 89(2): 93–104, doi: 10.1016/j.aquabot.2008.02.007

Fan Hangqing, Chen Guanghua, He Binyuan, et al. 2005. Coastal Wetland and Management of Shankou Mangroves (in Chinese). Beijing: China Ocean Press, 35–89

França M C, Francisquini M I, Cohen M C L, et al. 2014. Inter-proxy evidence for the development of the Amazonian mangroves during the Holocene. Vegetation History and Archaeobotany, 23(5): 527–542, doi: 10.1007/s00334-013-0420-4

Frederikse T, Landerer F, Caron L, et al. 2020. The causes of sea-level rise since 1900. Nature, 584(7821): 393–397, doi: 10.1038/s41586-020-2591-3

Gonneea M E, Paytan A, Herrera-Silveira J A. 2004. Tracing organic matter sources and carbon burial in mangrove sediments over the past 160 years. Estuarine, Coastal and Shelf Science, 61(2): 211–227, doi: 10.1016/j.ecss.2004.04.015

Guo Zhigang, Lin Tian, Zhang Gan, et al. 2007. The sedimentary fluxes of polycyclic aromatic hydrocarbons in the Yangtze River Estuary coastal sea for the past century. Science of the Total Environment, 386(1–3): 33–41, doi: 10.1016/j.scitotenv.2007.07.019

Hapsari K A, Biagioni S, Jennerjahn T C, et al. 2017. Environmental dynamics and carbon accumulation rate of a tropical peatland in Central Sumatra, Indonesia. Quaternary Science Reviews,

169: 173–187, doi: 10.1016/j.quascirev.2017.05.026
Hatje V, Masqué P, Patire V F, et al. 2021. Blue carbon stocks, accumulation rates, and associated spatial variability in Brazilian mangroves. Limnology and Oceanography, 66(2): 321–334, doi: 10.1002/lno.11607
Herbeck L S, Unger D, Krumme U, et al. 2011. Typhoon-induced precipitation impact on nutrient and suspended matter dynamics of a tropical estuary affected by human activities in Hainan, China. Estuarine, Coastal and Shelf Science, 93(4): 375–388, doi: 10.1016/j.ecss.2011.05.004
Huang Xuesong, Kuang Xueyuan, Qin Zhengrong, et al. 2007. Multi-time-scale variations of recent centenary series of temperature and precipitation in Guangxi of China. Advances in Climate Change Research (in Chinese), 3(6): 362–367
Jennerjahn T C. 2012. Biogeochemical response of tropical coastal systems to present and past environmental change. Earth-Science Reviews, 114(1–2): 19–41, doi: 10.1016/j.earscirev.2012.04.005
Jennerjahn T C, Ittekkot V. 2002. Relevance of mangroves for the production and deposition of organic matter along tropical continental margins. Naturwissenschaften, 89(1): 23–30, doi: 10.1007/s00114-001-0283-x
Krishnaswamy S, Lal D, Martin J M, et al. 1971. Geochronology of lake sediments. Earth and Planetary Science Letters, 11(1–5): 407–414, doi: 10.1016/0012-821X(71)90202-0
Kristensen E, Bouillon S, Dittmar T, et al. 2008. Organic carbon dynamics in mangrove ecosystems: a review. Aquatic Botany, 89(2): 201–219, doi: 10.1016/j.aquabot.2007.12.005
Kusumaningtyas M A, Hutahaean A A, Fischer H W, et al. 2019. Variability in the organic carbon stocks, sources, and accumulation rates of Indonesian mangrove ecosystems. Estuarine, Coastal and Shelf Science, 218: 310–323, doi: 10.1016/j.ecss.2018.12.007
Lamb A L, Wilson G P, Leng M J. 2006. A review of coastal palaeoclimate and relative sea-level reconstructions using $\delta^{13}C$ and C/N ratios in organic material. Earth-Science Reviews, 75(1–4): 29–57, doi: 10.1016/j.earscirev.2005.10.003
Li Zhen, Zhang Zhiying, Li Jie, et al. 2008. Pollen distribution in surface sediments of a mangrove system, Yingluo Bay, Guangxi, China. Review of Palaeobotany and Palynology, 152(1–2): 21–31, doi: 10.1016/j.revpalbo.2008.04.001
MacKenzie R A, Foulk P B, Klump J V, et al. 2016. Sedimentation and belowground carbon accumulation rates in mangrove forests that differ in diversity and land use: a tale of two mangroves. Wetlands Ecology and Management, 24(2): 245–261, doi: 10.1007/s11273-016-9481-3
Matos C R L, Berrêdo J F, Machado W, et al. 2020. Carbon and nutrient accumulation in tropical mangrove creeks, Amazon region. Marine Geology, 429: 106317, doi: 10.1016/j.margeo.2020.106317
Mcleod E, Chmura G L, Bouillon S, et al. 2011. A blueprint for blue carbon: toward an improved understanding of the role of vegetated coastal habitats in sequestering CO_2. Frontiers in Ecology and the Environment, 9(10): 552–560, doi: 10.1890/110004
Meng Xianwei, Xia Peng, Li Zhen, et al. 2016. Mangrove degradation and response to anthropogenic disturbance in the Maowei Sea (SW China) since 1926 AD: Mangrove-derived organic matter and pollen. Organic Geochemistry, 98: 166–175, doi: 10.1016/j.orggeochem.2016.06.001
Meng Xianwei, Xia Peng, Li Zhen, et al. 2017. Mangrove development and its response to Asian monsoon in the Yingluo Bay (SW China) over the last 2000 years. Estuaries and Coasts, 40(2): 540–552, doi: 10.1007/s12237-016-0156-3
Meng Xianwei, Zhang Chuangzhi. 2014. Basic Situations of Marine Environment and Resources in Guangxi (in Chinese). Beijing: China Ocean Press, 5–22
Nellemann C, Corcoran E, Duarte C, et al. 2009. Blue Carbon: the Role of Healthy Oceans in Binding Carbon. Norway: United Nations Environment Programme, 11–65
Osland M J, Day R H, Hall C T, et al. 2017. Mangrove expansion and contraction at a poleward range limit: climate extremes and land-ocean temperature gradients. Ecology, 98(1): 125–137, doi: 10.1002/ecy.1625
Robbins J A, Edgington D N. 1975. Determination of recent sedimentation rates in Lake Michigan using Pb-210 and Cs-137. Geochimica et Cosmochimica Acta, 39(3): 285–304, doi: 10.1016/0016-7037(75)90198-2
Sanchez-Cabeza J A, Ruiz-Fernández A C. 2012. ^{210}Pb sediment radiochronology: an integrated formulation and classification of dating models. Geochimica et Cosmochimica Acta, 82: 183–200, doi: 10.1016/j.gca.2010.12.024
Sanders C J, Smoak J M, Naidu A S, et al. 2010. Organic carbon burial in a mangrove forest, margin and intertidal mud flat. Estuarine, Coastal and Shelf Science, 90(3): 168–172, doi: 10.1016/j.ecss.2010.08.013
Sasmito S D, Kuzyakov Y, Lubis A A, et al. 2020. Organic carbon burial and sources in soils of coastal mudflat and mangrove ecosystems. CATENA, 187: 104414, doi: 10.1016/j.catena.2019.104414
Smoak J M, Breithaupt J L, Smith III T J, et al. 2013. Sediment accretion and organic carbon burial relative to sea-level rise and storm events in two mangrove forests in Everglades National Park. CATENA, 104: 58–66, doi: 10.1016/j.catena.2012.10.009
Tateda Y, Nhan D D, Wattayakorn G, et al. 2005. Preliminary evaluation of organic carbon sedimentation rates in Asian mangrove coastal ecosystems estimated by ^{210}Pb chronology. Radioprotection, 40: S527–S532, doi: 10.1051/radiopro:2005s1-077
Veettil B K, Ward R D, Quang N X, et al. 2019. Mangroves of Vietnam: Historical development, current state of research and future threats. Estuarine, Coastal and Shelf Science, 218: 212–236, doi: 10.1016/j.ecss.2018.12.021
Woodroffe C D, Rogers K, McKee K L, et al. 2016. Mangrove sedimentation and response to relative sea-level rise. Annual Review of Marine Science, 8: 243–266, doi: 10.1146/annurev-marine-122414-034025
Xia Peng, Meng Xianwei, Li Zhen, et al. 2015. Mangrove development and its response to environmental change in Yingluo Bay (SW China) during the last 150 years: stable carbon isotopes and mangrove pollen. Organic Geochemistry, 85: 32–41, doi: 10.1016/j.orggeochem.2015.04.003
Xia Peng, Meng Xianwei, Zhang Yao, et al. 2021. The potential of mangrove-derived organic matter in sediments for tracing mangrove development during the holocene. Estuaries and Coasts, 44(4): 1020–1035, doi: 10.1007/s12237-020-00826-w
Xue Bo, Yan Chongling, Lu Haoliang, et al. 2009. Mangrove-derived organic carbon in sediment from Zhangjiang Estuary (China) mangrove wetland. Journal of Coastal Research, 2009(254): 949–956
Yang Juan, Gao Jay, Liu Baolin, et al. 2014. Sediment deposits and organic carbon sequestration along mangrove coasts of the Leizhou Peninsula, southern China. Estuarine, Coastal and Shelf Science, 136: 3–10, doi: 10.1016/j.ecss.2013.11.020
Zhang Yao, Meng Xianwei, Bai Yazhi, et al. 2021. Sources and features of particulate organic matter in tropical small mountainous rivers (SW China) under the effects of anthropogenic activities. Ecological Indicators, 125: 107471, doi: 10.1016/j.ecolind.2021.107471